AIAA 2006-6504

BOOM AND RECEPTACLE AUTONOMOUS AIR REFUELING USING A VISUAL PRESSURE SNAKE OPTICAL SENSOR

James Doebbler and John Valasek

Texas A&M University, College Station, TX 77843-3141

Mark Monda and Hanspeter Schaub

Virginia Tech, Blacksburg, VA 24061-0203

AIAA Guidance, Navigation and Control Conference
Keystone, CO, August 21-24, 2006

Boom and Receptacle Autonomous Air Refueling Using a Visual Pressure Snake Optical Sensor

James Doebbler[*] and John Valasek[†]

Texas A&M University, College Station, TX 77843-3141

Mark J. Monda [‡] and Hanspeter Schaub [§]

Virginia Polytechnic Institute, Blacksburg, VA 24061-0203

Autonomous in-flight air refueling is an important capability for the future deployment of unmanned air vehicles, since they will likely be ferried in flight to overseas theaters of operation instead of being shipped unassembled in containers. This paper introduces a vision sensor based on active deformable contour algorithms, and a relative navigation system that enables precise and reliable boom and receptacle autonomous air refueling for non micro sized unmanned air vehicles. The sensor is mounted on the tanker aircraft near the boom, and images a single passive target image painted near the refueling receptacle on the receiver aircraft. Controllers are developed for the automatic control of the refueling boom, and for the station keeping controller of the receiver aircraft. The boom controller is integrated with the active deformable contour sensor system, and feasibility of the total system is demonstrated by simulated docking maneuvers in the presence of various levels of turbulence. Results indicate that the integrated sensor and controller enables precise boom and receptacle air refueling, including consideration of realistic measurement errors and disturbances.

I.   Introduction

There are currently two approaches used for air refueling. The probe-and-drogue refueling system is the standard for the United States Navy and the air forces of most other nations. In this method, the tanker trails a hose with a flexible "basket", called a drogue, at the end. The drogue is aerodynamically stabilized. It is the responsibility of the pilot of the receiver aircraft to maneuver the receiver's probe into the drogue. This method is used for small, agile aircraft such as fighters because both the hose and drogue are flexible and essentially passive during re-fueling; a human operator is not required on the tanker.[1–3] Autonomous in-flight refueling using a probe-and-drogue system is basically a docking situation that probably requires 2 cm accuracy in the relative position of the refueling probe (from the receiving aircraft) with respect to the drogue (from the tanker) during the end-game. This specification is based on the geometry of the existing probe and drogue hardware, and the need to ensure that the tip of the probe contacts only the inner sleeve of the receptacle and not the more lightly constructed and easily damaged shroud.[4]

The United States Air Force uses the flying boom developed by Boeing. The boom approach is supervised and controlled by a human operator from a station near the rear of the tanker aircraft, who is responsible for "flying" the boom into the refueling port on the receiver aircraft. In this method, the job of the receiver aircraft is to maintain proper refueling position with respect to the tanker, and leave the precision control function to the human operator in the tanker.[2]

---

[*]Graduate Research Assistant, Flight Simulation Laboratory, Aerospace Engineering Department. Student Member AIAA. james.doebbler@tamu.edu

[†]Associate Professor and Director, Flight Simulation Laboratory, Aerospace Engineering Department. Associate Fellow AIAA. valasek@tamu.edu

[‡]Graduate Research Assistant, Aerospace and Ocean Engineering Department. Student Member AIAA. mjmonda@vt.edu

[§]Assistant Professor, Aerospace and Ocean Engineering Department. Member AIAA. schaub@vt.edu

American Institute of Aeronautics and Astronautics

Figure 1. B-1B Lancer Refueling From a KC-10 Extender Using the Boom and Receptacle Method

Regardless of the type of autonomous refueling to be conducted, the maturation of the technology requires several issues to be addressed, the most fundamental being the lack of sufficiently accurate/reliable relative motion sensors.[5] Some methods that have been considered for determining relative position in a refueling scenario include measurements derived from the Global Positioning System (GPS), measurements derived from both passive and active machine vision, and visual servoing with pattern recognition software.[6-10] GPS measurements have been made with 1 cm to 2 cm accuracy for formation flying, but problems associated with lock-on, integer ambiguity, low bandwidth, and distortions due to wake effects from the tanker present challenges for application to in-flight refueling. Pattern recognition codes are not sufficiently reliable in all lighting conditions, and with adequate fault tolerance, may require large amounts of computational power in order to converge with sufficient confidence to a solution.[6-8]

Machine vision based techniques use optical markers to determine relative orientation and position of the tanker and the UAV. The drawback of the machine vision based techniques is the assumption that all the optical markers are always visible and functional. Reference[11] proposes an alternative approach where the pose estimation does not depend on optical markers but on Feature Extraction methods, using specific corner detection algorithms. Special emphasis was placed on evaluating the accuracy, required computational effort, and robustness to different sources of noise. Closed loop simulations were performed using a detailed Simulink-based simulation environment to reproduce boom and receptacle docking maneuvers.

Another approach is an active vision based navigation system called VisNav. VisNav provides a high precision six degree-of-freedom information for real-time navigation applications.[12-14] VisNav is a cooperative vision technology in which a set of beacons mounted on a target body (e.g., the receiver aircraft) are supervised by a VisNav sensor mounted on a second body (e.g., the boom). VisNav structures the light in the frequency domain, analogous to radar, so that discrimination and target identification are near-trivial even in a noisy ambient environment. Controllers which use the VisNav sensor have been developed and evaluated specifically for probe and drogue autonomous air refueling.[15-22] In principle, the VisNav system could work with legacy boom and receptacle refueling systems since the only major equipment changes are mounting the VisNav sensor to the boom and attaching four or more Light Emitting Diode (LED) beacon lights to the forebody of the receiver aircraft, or vice versa.

Another class of sensing methods are the active deformable contour algorithms. These methods segment the target area of the image by having a closed, non-intersecting contour

American Institute of Aeronautics and Astronautics

iterate across the image and track a target. In 1987 Kass et al. proposed the original active deformable model to track targets within an images stream.[23] They are also known as visual snakes. For application to the end game docking problem of autonomous air refueling, a visual snake optical sensor mounted on the boom would acquire and track a geometric pattern painted on the receiver aircraft, and develop a relative navigation solution which is then passed to a boom control system. This approach does not use pattern recognition, is passive, and highly robust in various lighting conditions. Although it does not provide six degree-of-freedom data, this is not a penalty for boom and receptacle autonomous refueling since the boom requires only two rotations and one translation to successfully engage the receptacle.

Figure 2. Conceptual Picture of a KC-135 Refueling a Predator UAV

Referring to Fig. 2, the system proposed in this paper is comprised of a receiver aircraft (in this case an Unmanned Air Vehicle (UAV)) equipped with a GPS sensor, and an onboard flight controller which permits it to station keep in a 3D box of specified dimensions, relative to the tanker aircraft. The receiver aircraft has a visual docking target painted on its forebody, similar to the target painted on the forebody of the B-1B in Fig. 1. The tanker aircraft is equipped with two sensors dedicated to autonomous air refueling. The first sensor accurately measures the angular position of the boom at the pivot point, as well as the length of the boom, thereby providing a measurement of the tip of the boom. The second sensor is the visual pressure snake sensor, which is mounted on the rear of the tanker and oriented so that it possesses a clear, unobstructed field-of-view of the visual docking target painted on the receiver aircraft's forebody. For night refueling operations, the visual target painted on the receiver aircraft is illuminated by a light installed on the tanker. An automatic control system for the refueling boom receives estimates of the refueling receptacle position from the visual pressure snakes sensor, and steers the boom tip into it. There are no controller commands which would require a high speed, high bandwidth data link being passed between the tanker and receiver aircraft. A communication link handles initiation and termination of the refueling sequence.

This paper develops a vision based relative navigation system that uses a visual pressure snakes optical sensor integrated with an automatic boom controller for autonomous boom and receptacle air refueling. The capability of this system to accurately estimate

American Institute of Aeronautics and Astronautics

the position of the receptacle, and then automatically steer the boom into it in light and moderate atmospheric turbulence conditions, is demonstrated using non real-time simulation. Detailed software models of the optical sensor system are integrated with the boom and station keeping controllers, and evaluated with refueling maneuvers on a six degree-of-freedom simulation. Test cases consisting of initial positioning offsets in still air, and maneuvers in turbulence, are used to evaluate the combined performance of the optical sensor, boom controller, and station keeping controller system. For the refueling scenario investigated here, only the end-game docking maneuver is considered. It is assumed that the tanker and receiver have already rendezvoused, and that the tanker is flying straight ahead at constant speed. The receiver aircraft is positioned aft of the tanker in trimmed flight, and an onboard flight controller maintains position within a 3D box relative the to the tanker.

The paper is organized as follows. First the basic working principles and components of the visual pressure snakes navigation sensor is presented in Section II, detailing the algorithm and navigation solution, performance, forced perspective target setup, and error sensitivities. This is followed by a description of the boom model in Section III, and derivation of the Proportional-Integral-Filter optimal Nonzero Setpoint controller(PIF-NZSP) boom control law in Section IV. The receiver aircraft station keeping controller is developed in Section V, and the tanker and receiver aircraft linear state-space models are developed in Section VI. In Section VII, test cases using the Dryden gust model with light and moderate turbulence is used to assess system performance and disturbance accommodation characteristics in the presence of exogenous inputs. Finally, conclusions and recommendations for further work are presented in Section VIII.

II.   Visual Pressure Snakes Navigation Sensor

A.   Visual Relative Motion Sensing

A critical technology for autonomous air refueling is a sensor for measuring the relative position and orientation between the receiver aircraft and the tanker aircraft. Because rapid control corrections are required for docking, especially in turbulence, the navigation sensor must provide accurate, high-frequency updates. The proposed autonomous refueling method uses color statistical pressure snakes[24–26] to sense the relative position of the target aircraft with respect to the tanker craft. Statistical pressure snakes methods, or visual snakes, segment the target area of the image and track the target with a closed, non-intersecting contour. Hardware experiments verify that visual snakes can provide relative position measurements at rates of 30 Hz even using a standard, off-the-shelf 800 MHz processor.[27] The visual snake provides not only information about the target size and centroid location, but also provides some information about the target shape through the principal axes lengths. The proposed relative motion sensor employs a simple, rear-facing camera mounted on the tanker aircraft, while the receiving vehicle has a visual target painted on its forebody near the refueling receptacle. Because the nominal relative position between the aircraft during a refueling maneuver is fixed, the relative heading and range to the receiver aircraft is accurately determined from the target image center of mass and principal axes sizes.

B.   Visual Snake Algorithm

In 1987 Kass *et al.* proposed the original active deformable model to track targets within an images stream.[28] Also referred to as a visual snake, the parametric curve is of the form

$$S(u) = I(x(u), y(u))', \qquad u = [0, 1] \tag{1}$$

where I is the stored image. This curve is placed into an image-gradient-derived potential field and allowed to change its shape and position in order to minimize the energy E along the length of the curve $S(u)$. The energy function is expressed as:[28]

$$E = \int_0^1 \Big[E_{\mathbf{int}}(S(u)) + E_{\mathbf{img}}(S(u), I) \Big] \mathbf{d}u \tag{2}$$

where $E_{\mathbf{int}}$ is the internal energy defined as

$$E_{\mathbf{int}} = \frac{\alpha}{2} \left| \frac{\partial}{\partial u} S(u) \right|^2 + \frac{\beta}{2} \left| \frac{\partial^2}{\partial u^2} S(u) \right|^2 \mathbf{d}u \tag{3}$$
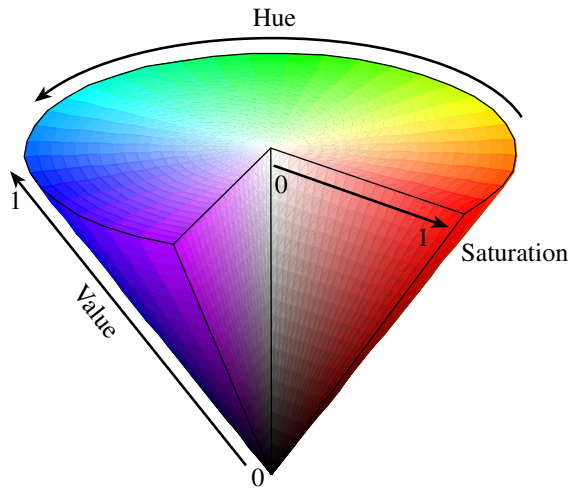
American Institute of Aeronautics and Astronautics

Figure 3. Conic Illustration of the Hue-Saturation-Value (HSV) Color Space.

and $E_{\mathbf{img}}$ is the image pressure function. The free weighting parameters α and β enforce tension and curvature requirements of the curve $S(u)$.

The active deformable models can be divided into two groups:[29] parametric models (snakes)[24, 28] and level-set models (geometric contours).[30] The original Kass snake formulation is a parametric snake solution. However, it is very difficult to tune and has several well document limitations. For example, the target contours tend to implode in the presence of weak gradients. While level sets models show excellent segmentation and robustness capabilities, they remain challenging to implement in real-time applications. Instead, this work will use modified parametric snake formulations proposed by Ivins and Porrill.[31] Here a pressure function is introduced which computes the statistical similarity of pixels values around a control point to create a pressure force which drives the snake toward the target boundaries. The new energy function is given by

$$E = \int_0^1 \Big[E_{\mathbf{int}}(S(u)) + E_{\mathbf{pres}}(S(u)) \Big] \mathrm{d}u \tag{4}$$

where the pressure energy function $E_{\mathbf{pres}}$ is

$$E_{\mathbf{pres}} = \rho \left(\partial S / \partial u \right)^{\perp} (\epsilon - 1) \tag{5}$$

and ϵ is statistical error measure of the curve $S(u)$ covering the target. Perrin and Smith suggest to replace the $E_{\mathbf{int}}$ expression with a single term that maintains a constant third derivative.[24] This simplified formulation includes an even snake point spacing constraint. The resulting algorithm does not contain the difficult to tune tension and curvature forces terms, yielding an easier to use and more efficient parametric snake algorithm.

Numerical efficiency is critical when trying to apply visual snakes to the control of autonomous vehicles. A fast snake point cross-over check algorithm is implemented which yields significant speed improvements for larger sets of snake points.[26] Further, to provide robustness to lighting variations, Schaub and Smith propose a new image error function:[25]

$$\epsilon = \sqrt{ \left(\frac{p_1 - \tau_1}{k_1 \sigma_1} \right)^2 + \left(\frac{p_2 - \tau_2}{k_2 \sigma_2} \right)^2 + \left(\frac{p_3 - \tau_3}{k_3 \sigma_3} \right)^2 }$$

where p_i are local average pixel color channel values, τ_i are the target color channel values and σ_i are the target color channel standard deviations. The gains k_i are free to chosen. The image RGB colors are mapped into the Hue-Saturation-Value color space illustrated in Figure 3. By choosing appropriate gains k_i, the visual snake can track targets with significant variations in target saturation and shading.

In Reference 25 target definition enhancements are performed to move beyond the typical grey-scale definitions to utilize the full three-dimensional color space as illustrated in Figure 4. Note the robustness of this prototype algorithm to drastic changes in lighting

American Institute of Aeronautics and Astronautics
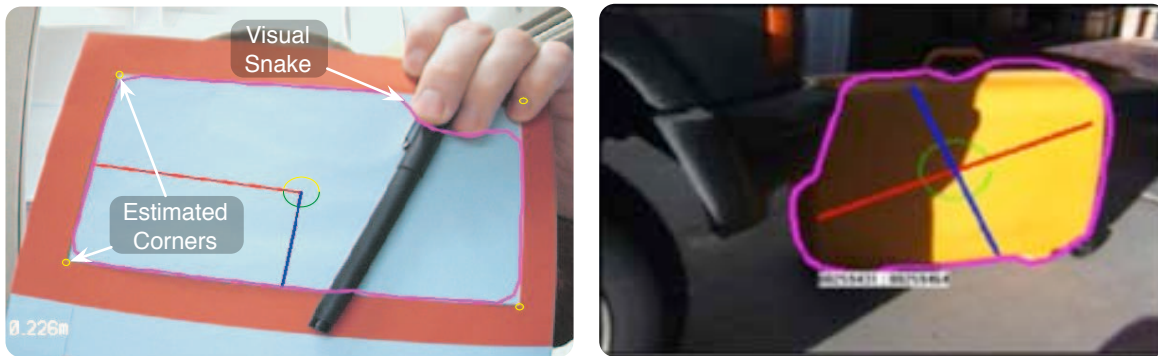
(a) Visual Snake Tracking a Partially Obscured Square Target and Estimating the Corner Locations[32]

(b) Visual Snake Tracking a Yellow Suit-Case Outdoors with Severe Lighting Variations[25]

Figure 4. Examples of the Identical Visual Snake Algorithm Tracking Different Targets. Each target is selected by double-clicking on it within the image.

variations. Here the same algorithm and gains are used to track the indoor square target, as well as an outdoor yellow suitcase. The visual snake forms a closed contour about the target and is not disturbed by the presence of the black pen in Figure 4(a). The computational requirement of the statistical pressure snakes is relatively low compared to conventional image processing techniques such as image eigenvalue analysis. Real-time 30 Hz image processing is feasible with a 800 MHz processor without additional hardware acceleration. The computational efficiency of the visual tracking algorithm determines the performance and control bandwidth of the relative motion tracking solution.

Using the hue-saturation-value (HSV) color space in particular, robust tracking results were demonstrated in hardware by varying lighting conditions. Figure 4(b) illustrates how an operator was able to click on the yellow suitcase in the image, and the visual snake is able to track it. Besides computing the target centroid location, the image principle axes can be computed from the 2nd area moments and be used to track the camera rotation about its bore-sight. By defining the statistical target color properties in HSV space, the harsh shadow being cast across the target does not confuse the visual snake. This example illustrates the exciting potential of using this visual sensing method in space where dramatic lighting conditions exist. For the autonomous aircraft refueling application, a visual target is painted on the front of the aircraft. As the fueling rod is extended, the fuel docking port heading and distance of the chaser aircraft is sensed by employing the visual snake algorithm.

C. Visual Snake Performance

This section discusses the performance of the visual snake algorithm as a relative navigation sensing technique. The accuracy of this sensing method is determined primarily by the accuracy of the target area, COM, and principal axis length measurements. We therefore seek to compare the measured values for these parameters with the true values. However, determining the true values in real world test conditions is extremely challenging. Moreover, due to issues related to target colors, pixelation at the target image boundary, and lens distortion specific to a particular camera/lens system, the performance would only be indicative of a particular test case, rather than the algorithm as a whole. We therefore confine this discussion to an ideal test case that shows the performance of the algorithm itself. This ideal test case represents an upper bound on performance of the snake algorithm as a visual sensor.

To construct the ideal test case, a "perfect" target of known size, shape, location, and pure color is drawn on the video image frame before processing with the visual snake. An example frame shot at high magnification is seen in Figure 5. Note the perfectly crisp color boundaries in the ideal test image, in contrast to the boundaries seen in an image taken with a real camera. Performance data is taken for a rectangular target with a width of 200 pixels. The visual snake is started 20 times and a total of 5000 image frames are captured. The transients associated with the snake first converging to the target are removed, so the
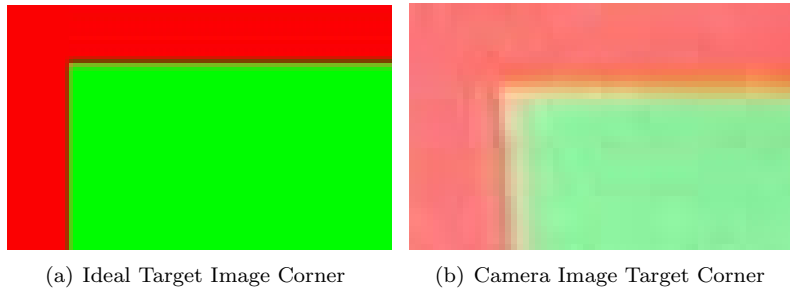
American Institute of Aeronautics and Astronautics

(a) Ideal Target Image Corner   (b) Camera Image Target Corner

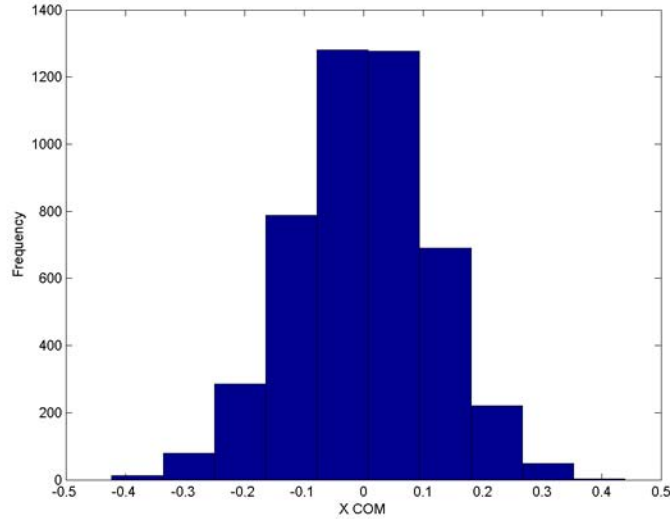**Figure 5. Zoomed View of a Target Edge for an Ideal Test Image and a Camera Image.**

Figure 6. Histogram of X COM Measurement Error from the Visual Snake Algorithm with an Elliptical Ideal Test Image.

remaining data represents "steady-state" performance.

First, note that the COM and principal axis length measurement errors resulting from the visual snake are approximately Gaussian, as seen in Figure 6. This implies that combining the visual snake with a Kalman filter might enhance the accuracy of the measurements.

In air refueling problem where the vehicle attempts to maintain a constant range and orientation to a target, the visual snake can be "calibrated" about this nominal state, and better performance can be obtained. Table 1 shows the performance for a rectangular target at an image size of 200 pixels. The bias errors are corrected so that the mean values match the true values for this image size. The values in Table 1 represent an upper-bound on the performance of this visual snake algorithm as a relative pose sensor.

Table 1. Statistically Averaged Snake Performance for an Elliptical Target of Size 200 Pixels

Description	Pixels	Percentage
$\sigma_{\mathrm{COM_x}}$	0.1088	0.0544%
σ_{Length}	0.1347	0.0674%

D. Forced Perspective Target Setup

To use visual snakes as part of an air refueling system, a camera and a visual target must be placed on the tanker and receiver aircraft, respectively. The visual target should be placed
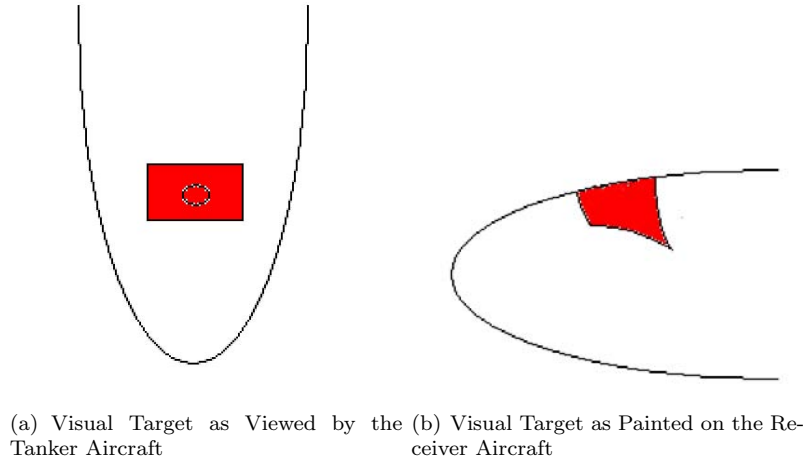
American Institute of Aeronautics and Astronautics

(a) Visual Target as Viewed by the Tanker Aircraft

(b) Visual Target as Painted on the Receiver Aircraft

Figure 7. Illustration of Forced Perspective Showing Visual Targets as Seen by the Tanker and as Painted on the Receiver.

as close as possible to the receiver aircraft receptacle. This greatly reduces any position errors that might be introduced by the inability of the visual snake sensor to measure the full 3 DOF orientation of the receiver aircraft.

The target image COM location is used to determine the 2D relative heading to the target, and the principal axis sizes are used to determine range. From these measurements, the relative position of the receptacle is determined. For particular target shapes, the principal axis sizes can be determined from the target image moments. However, when using the target area, first, and second moments, this only holds for target shapes parameterizable by two measurements and for which there is an analytical relationship between the those parameters and the moments. Examples include a rectangle, which is parameterized by its length and width, or an ellipse, parameterized by its semi-major and semi-minor axes. For an arbitrary target shape however, the relationship cannot be determined. Therefore, the target image should appear as a rectangle or an ellipse in the camera image plane.

However in general, the camera image plane is not parallel to the plane on which the visual target is drawn, which means that the target image appears skewed in the camera plane. For example, a rectangle painted on the aircraft appears as a trapezoid in the camera image plane. Moreover, it is not guaranteed that a planar surface can be found in proximity to the refueling receptacle. Therefore, simply painting a visual target of the desired shape on the aircraft is not a feasible solution.

To make the target image, which is painted on a curved surface, appear as a desired shape in the camera image plane, we suggest using forced perspective. This technique, often employed by artists, consists of painting the target image so that it appears "correct" from some desired viewing position and orientation. This is illustrated in Figure 7. It is noted that the image is only correct when viewed from the nominal pose, and it appears skewed when viewed from any other pose. However, in this air refueling application, this is not a significant problems, because the air refueling operation can only take place when the aircraft are at or very near their nominal positions. The visual snake measurement errors caused by slight deviations from the nominal relative pose between the aircraft are analyzed and discussed in Section E.

To find the shape that must be painted on the target to produce the desired camera image plane shape, rays are projected from the desired image shape on the camera plane through the focal point. The intersection of those rays and the receiver aircraft surface generates the contour that appears as the desired shape in the camera image plane.

E.   Sensitivity Analysis

As discussed in the previous section, the use of forced perspective implies that the target image is only the "correct" shape when the relative pose between the aircraft is the nominal pose. Perturbations from the nominal pose skew the target image shape, and the resulting

American Institute of Aeronautics and Astronautics

Table 2. Range Error and Heading Error Sensitivity to Perturbations from Nominal Position in the air Refueling Visual Position Sensing Simulation

Axis	Range Error Sensitivity (m/m)	Heading Error Sensitivity (deg./m)
X	0.8756	0.0569
Y	0.0169	0.0009
Z	-0.5232	0.0372

Table 3. Range Error and Heading Error Sensitivity to Perturbations from Nominal Orientation in the air Refueling Visual Position Sensing Simulation

Angle	Range Error Sensitivity (m/deg.)	Heading Error Sensitivity (deg./deg.)
Yaw	0.0011	0.1606
Pitch	-0.1228	0.0460
Roll	4.761×10^{-4}	0.1405

moments calculated from the snake contour change. The relative COM heading and range calculations are therefore corrupted when there are perturbations from the nominal pose.

A numerical simulation designed to identify the error between the visual snake-measured and true relative headings and ranges is developed. This simulation assumes that the visual target is coincident with the refueling receptacle. For this analysis, the visual snake is assumed to track the target perfectly. The calculated errors are due to the method of extracting the relative heading and range from a contour, not the visual snake tracking errors. Using this simulation, the sensitivity of the relative heading and range errors to small perturbations about the nominal position and orientation of the receiver aircraft are determined with finite-difference derivatives.

Tables 2 and 3 show the error sensitivity to position and orientation perturbations, respectively. Standard aircraft coordinate systems (X forward, Y toward the right wing, Z down) and 3-2-1 Euler Angles are used. The nominal range between the camera and the visual target is 10.7 m. Because the visual snake measurement error is not included, these values are the sensitivity of the algorithm itself, and represent an upper bound on the performance of the entire visual sensing method.

In Table 2, the sensitivities to Y position perturbations are much lower than the other axes. This is because the nominal position is assumed to be directly in line with the tanker aircraft. In Table 3, perturbations in pitch are seen to be strongly coupled with range errors, while roll and yaw perturbations are strongly coupled with heading errors.

III. Refueling Boom Model

The refueling boom is modeled as a rigid, telescoping rod with two angular degrees-of-freedom (pitch and yaw), and one translational degree-of-freedom. As shown in Figure 8, the boom is attached to the tanker aircraft with a resolute joint, with dimensions and weights taken from Ref.[11] c
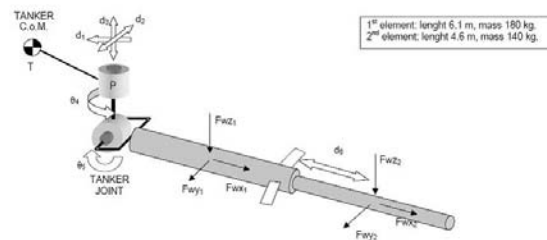

Figure 8. Refueling Boom Model Characteristics, Dimensions, and Weights[11]

American Institute of Aeronautics and Astronautics

IV.   Automatic Boom Controller

A.   Optimal Nonzero Set Point Controller

The optimal Nonzero Setpoint (NZSP) is a command structure which steers the plant to a terminal steady-state condition, with guaranteed tracking properties. It is used here to develop a simple yet functional baseline autonomous controller. For a linear time invariant system with n states and m controls,

$$
\begin{aligned}
\dot{\mathbf{x}} &= A\mathbf{x} + B\mathbf{u}; \qquad \mathbf{x}(0) = \mathbf{x}_0 \\
\mathbf{y} &= C\mathbf{x} + D\mathbf{u} \\
\mathbf{x} &\in \mathbb{R}^n, \quad \mathbf{u} \in \mathbb{R}^m, \quad \mathbf{y} \in \mathbb{R}^m
\end{aligned}
\tag{6}
$$

it is desired to command some of the initial outputs $\mathbf{y}$ to steady-state terminal output values $\mathbf{y}_m$ and keep them there as $t \to \infty$. If these terminal outputs are trim states, denoted by *, then at the terminal steady-state condition the system is characterized by

$$
\begin{aligned}
\dot{\mathbf{x}}^* &= A\mathbf{x}^* + B\mathbf{u}^* \equiv 0 \\
\mathbf{y}_m &= H\mathbf{x}^* + D\mathbf{u}^* \\
\mathbf{x}^* &\in \mathbb{R}^n, \quad \mathbf{u}^* \in \mathbb{R}^m, \quad \mathbf{y}_m \in \mathbb{R}^m
\end{aligned}
\tag{7}
$$

For guaranteed tracking, the number of commanded outputs $\mathbf{y}_m$ must be less than or equal to the number of controls m. Error states and error controls are defined as

$$
\begin{aligned}
\tilde{\mathbf{x}} &= \mathbf{x} - \mathbf{x}^* \\
\tilde{\mathbf{u}} &= \mathbf{u} - \mathbf{u}^*
\end{aligned}
\tag{8}
$$

where $\tilde{\mathbf{x}}$ and $\tilde{\mathbf{u}}$ are the error between the current state and control respectively, and the desired state and control respectively. The state equations can be written in terms of these error states as

$$
\begin{aligned}
\dot{\tilde{\mathbf{x}}} &= \dot{\mathbf{x}} - \dot{\mathbf{x}}^* = A\mathbf{x} + B\mathbf{u} - (A\mathbf{x}^* + B\mathbf{u}^*) \\
\dot{\tilde{\mathbf{x}}} &= A\tilde{\mathbf{x}} + B\tilde{\mathbf{u}}
\end{aligned}
\tag{9}
$$

with quadratic cost function to be minimized

$$
J = \frac{1}{2} \int_0^\infty \left[\tilde{\mathbf{x}}^T Q \tilde{\mathbf{x}} + \tilde{\mathbf{u}}^T R \tilde{\mathbf{u}} \right] dt
\tag{10}
$$

The optimal control which minimizes Eqn.10 is obtained by solving the matrix algebraic Riccati equation for infinite horizon

$$
PA + A^T P - PBR^{-1}B^T P + Q = 0
\tag{11}
$$

resulting in

$$
PA + A^T P - PBR^{-1}B^T P + Q = 0
\tag{12}
$$

A feedback control law in terms of the measured states is obtained by converting $\tilde{\mathbf{u}}$ back to $\mathbf{u}$, giving

$$
\mathbf{u} = (\mathbf{u}^* + K\mathbf{x}^*) - K\mathbf{x}
\tag{13}
$$

with $\mathbf{u}^*$ and $\mathbf{x}^*$ constants. They are solved for directly by inverting a quad partition matrix deduced from Eqn.7

$$
\begin{aligned}
\begin{bmatrix} A & B \\ H & D \end{bmatrix}^{-1} &= \begin{bmatrix} X_{11} & X_{12} \\ X_{21} & X_{22} \end{bmatrix} \\[6pt]
\begin{bmatrix} \mathbf{x}^* \\ \mathbf{u}^* \end{bmatrix} &= \begin{bmatrix} X_{11} & X_{12} \\ X_{21} & X_{22} \end{bmatrix} \begin{bmatrix} \mathbf{0} \\ \mathbf{y}_m \end{bmatrix}
\end{aligned}
\tag{14}
$$

and then solving for

$$
\begin{aligned}
\mathbf{x}^* &= X_{12}\mathbf{y}_m \\
\mathbf{u}^* &= X_{22}\mathbf{y}_m
\end{aligned}
\tag{15}
$$

American Institute of Aeronautics and Astronautics

Upon substitution in Eqn.13 the control law implementation equation becomes

$$\mathbf{u} = (X_{22} + KX_{12})\mathbf{y}_m - K\mathbf{x} \tag{16}$$

For the optimal control policy u to be admissible, the quad partition matrix must be invertible. Therefore, the equations for x* and u* must be linearly independent, and the number of outputs or states that can be driven to a constant value must be less than or equal to the number of available controls. An advantage of this controller is the guarantee of perfect tracking of a number of outputs equal to the number of controls, independent of the value of the gains, provided they are stabilizing. The gains can be designed using any desired technique, and only affect the transient performance, and not the guarantee of steady-state performance.

B.   Proportional-Integral-Filter Nonzero Setpoint Controller

The optimal NZSP controller developed above assumes that there are no exogenous inputs to the system. A controller for autonomous air refueling must possess both stability robustness and performance robustness, since it must operate in the presence of uncertainties, particularly unstructured uncertainties such as atmospheric turbulence. One technique to improve disturbance accommodation properties of a controller to exogenous inputs is to pre-filter the control commands with a low pass filter. This will also reduce the risk of Pilot Induced Oscillations (PIO) by reducing control rates. An effective technique which permits the performance of the pre-filter to be tuned with quadratic weights is the Proportional-Integral-Filter (PIF) methodology, which is an extension of the optimal NZSP developed in section IV. The resulting controller is termed Proportional Integral Filter - Nonzero Setpoint - Control Rate Weighting (PIF-NZSP), and is shown in Fig.9. For the present
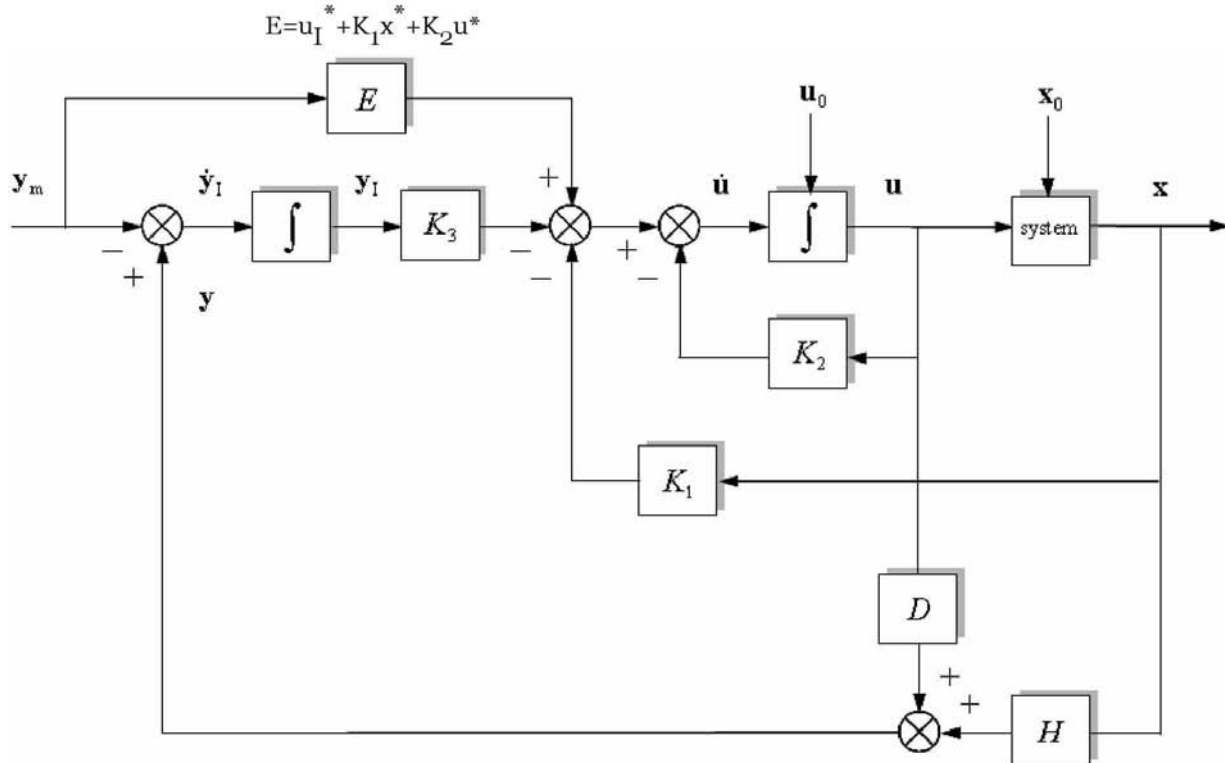

Figure 9. Proportional-Integral-Filter Nonzero Setpoint Block Diagram

problem a Type-1 system performance is desired, so integrator states $\mathbf{y}_I$ are created such that body-axis velocities u and v are integrated to x_{body} and y_{body} . To obtain the desired

American Institute of Aeronautics and Astronautics

filtering of the controls, the rates of the controls are also added as states u_1. The optimal NZSP is extended into the optimal PIF-NZSP structure by first creating the integral of the commanded error

$$\dot{\mathbf{y}}_I = \mathbf{y} - \mathbf{y}_m; \quad \dot{\mathbf{y}}_I \in \mathbb{R}^m \tag{17}$$

which upon substituting Eqn.6 becomes

$$
\begin{aligned}
\dot{\mathbf{y}}_I &= (H\mathbf{x} + D\mathbf{u}) - \mathbf{y}_m \\
&= H\mathbf{x} + D\mathbf{u} - H\mathbf{x}^* - D\mathbf{u}^* \\
&= H\tilde{\mathbf{x}} + D\tilde{\mathbf{u}}
\end{aligned} \tag{18}
$$

The augmented state-space system including the control rate states and integrated states is then

$$\dot{\tilde{\mathbf{x}}}_I = \begin{bmatrix} \dot{\tilde{\mathbf{x}}} \\ \dot{\tilde{\mathbf{u}}} \\ \dot{\tilde{\mathbf{y}} + I} \end{bmatrix} = \begin{bmatrix} A & B & 0 \\ 0 & 0 & 0 \\ H & D & 0 \end{bmatrix} \begin{bmatrix} \tilde{\mathbf{x}} \\ \tilde{\mathbf{u}} \\ \tilde{\mathbf{y}} + I \end{bmatrix} + \begin{bmatrix} 0 \\ I \\ 0 \end{bmatrix} \tilde{\mathbf{u}}_I \tag{19}$$

and the quadratic cost function to be minimized is

$$J = \frac{1}{2} \int_0^\infty \left[\tilde{\mathbf{x}}^T Q_1 \tilde{\mathbf{x}} + \tilde{\mathbf{u}}^T R \tilde{\mathbf{u}} + \tilde{\mathbf{u}}_I^T S_{rate} \tilde{\mathbf{u}}_I + \mathbf{y}_I^T Q_2 \mathbf{y_I} \right] dt \tag{20}$$

where the matrix $Q_1 \in \mathbb{R}^{n \times n}$ weights error states, the matrix $R \in \mathbf{R}^{m \times m}$ weights error controls, the matrix $S_{rate} \in \mathbb{R}^{m \times m}$ weights the control rates, and the matrix $Q_2 \in \mathbb{R}^{p \times p}$ weights the integrated states, with p the number of integrated states. Combining into the standard linear quadratic cost function form results in

$$J = \frac{1}{2} \int_0^\infty \left[\tilde{\mathbf{x}}_I^T \begin{bmatrix} Q_1 & 0 & 0 \\ 0 & R & 0 \\ 0 & 0 & Q_2 \end{bmatrix} \tilde{\mathbf{x}}_I + \tilde{\mathbf{u}}_I^T S_{rate} \tilde{\mathbf{u}}_I \right] dt \tag{21}$$

The minimizing control $\tilde{\mathbf{u}}_I$ is obtained from the solution to the matrix algebraic Riccati equation in infinite horizon

$$PA + A^T P - PBR^{-1}B^T P + Q = 0 \tag{22}$$

which results in

$$\tilde{\mathbf{u}}_I = -K_1 \tilde{\mathbf{x}} - K_2 \tilde{\mathbf{u}} - K_3 \mathbf{y}_I \tag{23}$$

Re-writing Eqn.23 in terms of the measured state variables produces

$$\mathbf{u}_I = (\mathbf{u}_I^* + K_1 \mathbf{x}^* + K_2 \mathbf{u}^*) - K_1 \mathbf{x} - K_2 \mathbf{u} - K_3 \mathbf{y}_I \tag{24}$$

with all * quantities constant, except for $\mathbf{u}_I^*$ which is equal to zero by the definition of steady-state. The constants $\mathbf{x}^*$ and $\mathbf{u}^*$ can be solved for by forming the quad partition matrix

$$\begin{bmatrix} A & B \\ H & D \end{bmatrix}^{-1} = \begin{bmatrix} X_{11} & X_{12} \\ X_{21} & X_{22} \end{bmatrix}$$

$$\begin{bmatrix} \mathbf{x}^* \\ \mathbf{u}^* \end{bmatrix} = \begin{bmatrix} X_{11} & X_{12} \\ X_{21} & X_{22} \end{bmatrix} \begin{bmatrix} \mathbf{0} \\ \mathbf{y}_m \end{bmatrix} \tag{25}$$

and solving for

$$
\begin{aligned}
\mathbf{x}^* &= X_{12}\mathbf{y}_m \\
\mathbf{u}^* &= X_{22}\mathbf{y}_m
\end{aligned} \tag{26}
$$

Upon substituting in Eqn.24 the control policy is

$$\mathbf{u}_I = (K_1 X_{12} + K_2 X_{22})\mathbf{y}_m - K_1 \mathbf{x} - K_2 \mathbf{u} - K_3 \mathbf{y}_I \tag{27}$$

Note that this PIF-NZSP control policy requires measurement and feedback of the control positions, in addition to full state feedback, in order to be admissible. As with the NZSP, the gains can be determined using any desired technique provided they are stabilizing. In this paper, the gains are designed using linear quadratic methods, thereby providing optimal gains.

American Institute of Aeronautics and Astronautics

V.   Receiver Aircraft Station Keeping Controller

The receiver aircraft is modeled as a linear, state-space, time-invariant system

$$
\begin{aligned}
\dot{\mathbf{x}} &= A\mathbf{x} + B\mathbf{u}; \qquad \mathbf{x}(0) = \mathbf{x}_0 \\
\mathbf{y} &= C\mathbf{x} + D\mathbf{u} \\
\mathbf{x} &\in \mathbb{R}^n, \quad \mathbf{u} \in \mathbb{R}^m, \quad \mathbf{y} \in \mathbb{R}^m
\end{aligned}
\tag{28}
$$

with state and control vectors defined as

$$
\begin{aligned}
\mathbf{x}^T &= \begin{bmatrix} \delta X & \delta Y & \delta Z & \delta u & \delta v & \delta w & \delta p & \delta q & \delta r & \delta\phi & \delta\theta & \delta\psi \end{bmatrix} \\
\mathbf{u}^T &= \begin{bmatrix} \delta ele & \delta\% pwr & \delta ail & \delta rud \end{bmatrix}
\end{aligned}
\tag{29}
$$

where $\delta()$ are the perturbations from the steady-state values, and the steady-state is assumed as steady, level, $1g$ flight. Here, δX, δY, δZ are perturbations in the inertial positions; δu, δv, δw are perturbations in the body-axis velocities; δp, δq, δr are perturbations in the body axis angular velocities; and $\delta\phi$, $\delta\theta$, $\delta\psi$ are perturbations in the Euler attitude angles. The control variables δele-elevator, $\delta\% pwr$-percentage power, δail-aileron and δrud-rudder are perturbations in the control effectors from the trim values.

The station keeping controller for maintaining the receiver aircraft position within the refueling box is a full-state feedback controller, designed using the optimal sampled-data regulator (SDR) technique.[33]

VI.   Tanker Aircraft and Receiver Aircraft Models

The receiver aircraft used for design and simulation purposes is a UAV called UCAV6. The UCAV6 simulation is used here because it is representative of the size and dynamical characteristics of a UAV. It is a roughly 60% scale AV-8B Harrier aircraft, with the pilot and support devices removed and the mass properties and aerodynamics adjusted accordingly. For the simulations presented here, all thrust vectoring capability was disabled. The simulation is a nonlinear, non real-time, six-degree-of-freedom computer code written in Microsoft Visual C++ 5.0. The UCAV6 longitudinal and lateral directional linear models used for both controller synthesis and simulation in this paper were obtained from the UCAV6 nonlinear simulation.[15] Atmospheric turbulence using the Dryden turbulence model, and the wake vortex effect from the tanker flowfield is included in the simulations.

The tanker aircraft state-space linear model uses Boeing 747 dynamics,[34] which are representative of a large multi-engine tankers of the KC-135 and KC-10 class. In the docking maneuvers investigated here, the rendezvous between tanker and receiver is assumed to have been achieved, with the receiver positioned in steady-state behind the tanker. The tanker aircraft is assumed to be flying in steady, level, 1-g straight line flight at constant velocity.

The dimensions of the receiver aircraft 3D refueling box are inspired by Ref.,[11] and are modified slightly to the values x± 0.25m, y± 0.75m, z± 0.5m.

VII.   Numerical Examples

The purpose of the examples is to demonstrate the performance of the integrated Visual Pressure Snakes sensor system and PIF-NZSP boom controller. The control objective is to dock the tip of the refueling boom into the receptacle located on the nose of the receiver aircraft, to an accuracy of ± 0.2m. The Visual Pressure Snake navigation solution provides the receptacle position and attitude estimates directly to the PIF-NZSP boom controller. The nominal position of the receiver aircraft is selected to be 9m behind and 8m below the aft end of the tanker aircraft. An important requirement is to ensure that the boom engages the receptacle with a forward velocity less than 0.5m/sec, so as to minimize impact damage. The visual snake optical sensor is mounted in the rear of the tanker aircraft above the boom, looking down on the receiver aircraft. The receptacle is configured with a painted on target consisting of a quadrilateral shape that appears as a square in the camera image plane when the receiver aircraft is at the nominal refueling position. The simulated flight condition is 250 knots true airspeed (KTAS) at 6,000m altitude, in both still and turbulent air. Four types of examples are presented. The first type invstigates

American Institute of Aeronautics and Astronautics

Visual Pressure Snake relative position estimates obtained from a simulation of the system that includes calibrations, range effects, corrections due to optical distortions, and sensor noise. Test Case I quantifies system performance in still air, while Cases II and III are in light turbulence and moderate turbulence respectively.

A. Relative Position Determination Results

This example shows the accuracy with which the visual snake can determine the 3D position of the receiver aircraft in favorable conditions, and is designed to show an upper limit on the sensor performance. The visual snake tracking errors are introduced to the numerical aircraft relative motion simulation to emulate the true performance of the visual sensing system. These simulations assume the receiver aircraft is at the nominal position, and, therefore do not include the effects of wind gusts, controls, *etc.*

The snake COM and principal axes size measurements are corrupted with Gaussian noise according to the characteristics determined in Section C. Because those values represent an ideal case where the target has perfectly crisp edges and pure colors, they noise levels were multiplied by a factor of two. This helps account for the non-crisp edges generated with real cameras, as seen in Figure 5(b). These simulation results all assume that the aircraft are at the nominal relative orientation and range of 10.7 m. If this were not the case, these results would be further corrupted according to the sensitivities seen in Tables **2** and **3**.

Figure 10 shows the errors resolved in the range and heading directions (with the angular heading uncertainty converted to a position uncertainty). Table 4 shows the mean and standard deviations. The error in range greatly dominates the error in heading. In other words, this visual sensing method determines the target COM heading much more accurately than it determines the range to the target. The resulting "measurement error envelope" looks like long thin tube, as illustrated in Figure 11. The green lines represent the cone defined by the heading uncertainty, and the red region corresponds to the depth uncertainty. Both regions are extremely exaggerated for effect.
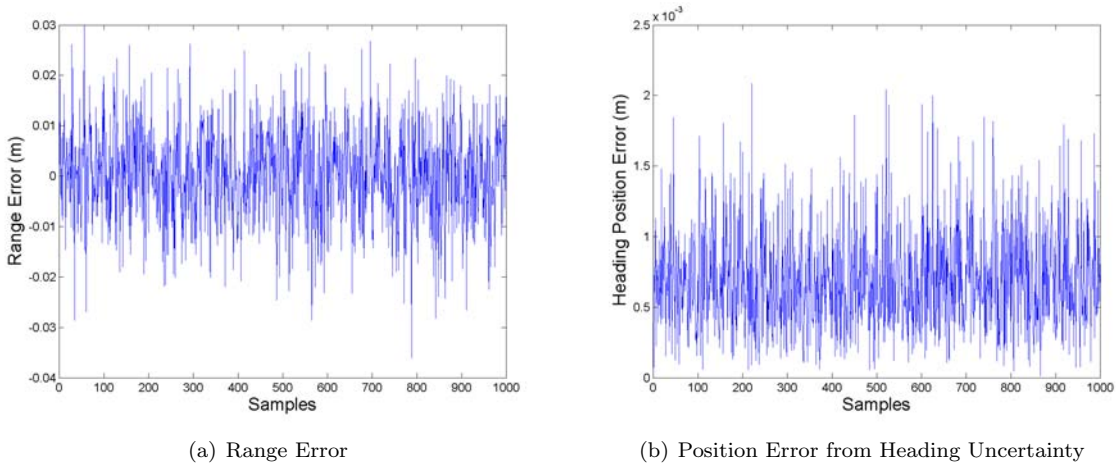

(a) Range Error

(b) Position Error from Heading Uncertainty

Figure 10. Range Error, Heading Error, and Heading Position Error for air Refueling Visual Position Sensing Simulation.

Table 4. Error Magnitude, Range Error, and Heading Error Data from air Refueling Visual Position Sensing Simulation.

Quantity	Mean	Standard Deviation
Error Magnitude (m)	0.0124	0.0057
Range Error (m)	6.2919×10^{-5}	0.0103
Heading Error (deg.)	0.0037	0.0020
Position Error from Heading Uncertainty (m)	6.89×10^{-4}	3.72×10^{-4}

American Institute of Aeronautics and Astronautics

Figure 11. Exaggerated Illustration of the Shape of the Range (Red) and Heading Errors (Green) from air Refueling Visual Position Sensing Simulation.

B. Case I. Still Air

For the still air case, the receiver aircraft remains at the nominal refueling position with the 3D box. The boom tip to receptacle position errors in Fig.12 show that the system smoothly and accurately docks the boom with the refueling receptacle. In Fig.13 the sensor output estimates of the UAV and the receptacle target are seen to closely follow the actual values.

Fig.14 shows that the boom controller smoothly steers the tip of the boom to the docking position. Finally, Fig.15 and Fig.16 show that the UAV is well behaved during the manuever, as all displacements and perturbations are small, and well damped. As shown in Fig.17, the control effector displacements are small, and all control rates (not shown) were well within limits.

C. Case II. Light Turbulence

For this case the receiver aircraft is subjected to light turbulence. The boom tip to receptacle position errors in Fig.18 show that the system smoothly and accurately docks the boom with the refueling receptacle. Although the boom trajectory lags the receiver aircraft trajectory, successful docking is achieved. In Fig.19 the sensor output estimates of the UAV and the receptacle target are seen to closely follow the actual values, in spite of the motion of the receiving aircraft relative to the sensor.

D. Case III. Moderate Turbulence

For this case the receiver aircraft is subjected to light turbulence. The boom tip to receptacle position errors in Fig.20 show that the system smoothly and accurately docks the boom with the refueling receptacle. Although the boom trajectory lags the receiver aircraft trajectory, successful docking is achieved. In Fig.21 the sensor output estimates of the UAV and the receptacle target are seen to closely follow the actual values, in spite of the motion of the receiving aircraft relative to the sensor.

VIII. Conclusions and Further Work

This paper presented the essential features of an optical sensor and boom controller for a vision based autonomous boom and receptacle air refueling system. Relative measurements are derived from a Visual Pressure Snake optical sensor system which makes use of active deformable contour algorithms, and associated relative navigation algorithms. Essential features of the optical sensor were developed and discussed, along with accuracies and sensitivities. An automatic boom control system was designed using the optimal
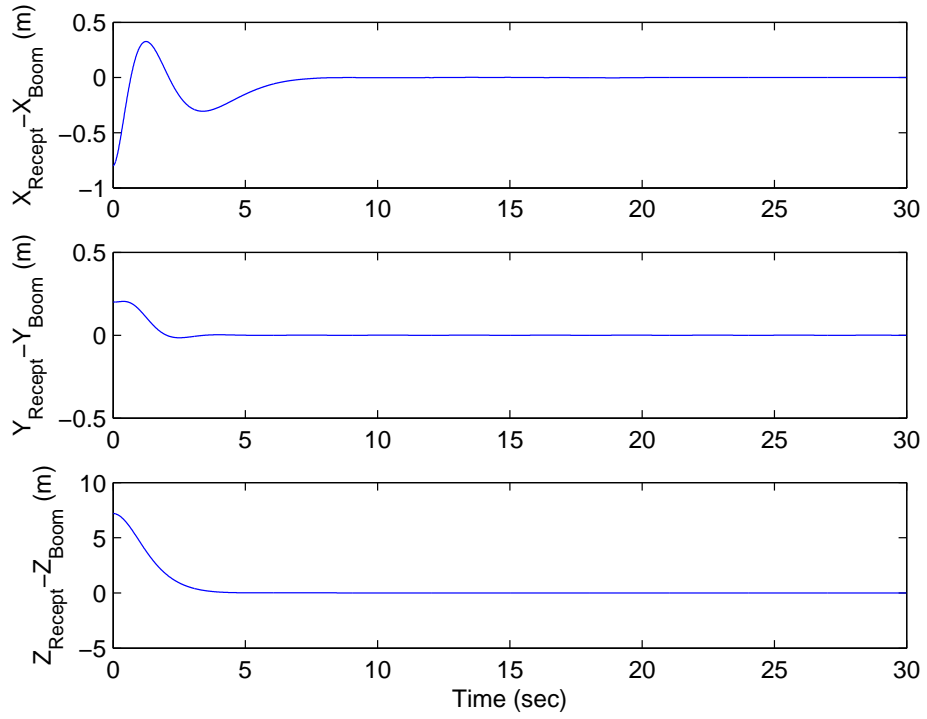
American Institute of Aeronautics and Astronautics

Figure 12. Case I Receptacle to Boom Tip Errors, Still Air
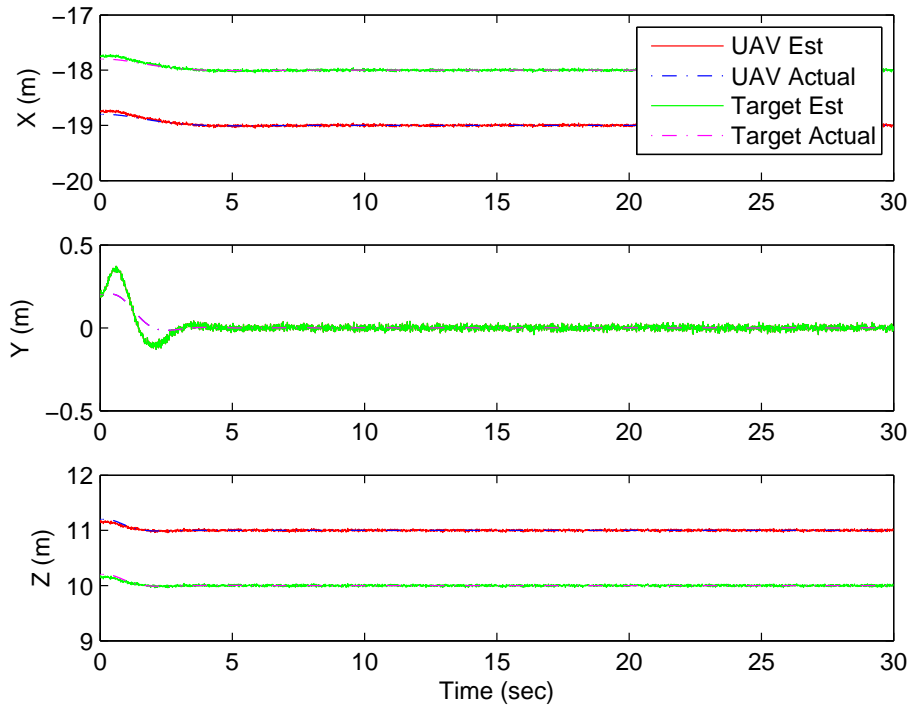
Figure 13. Case I Sensor Output Position Estimates, Still Air

American Institute of Aeronautics and Astronautics

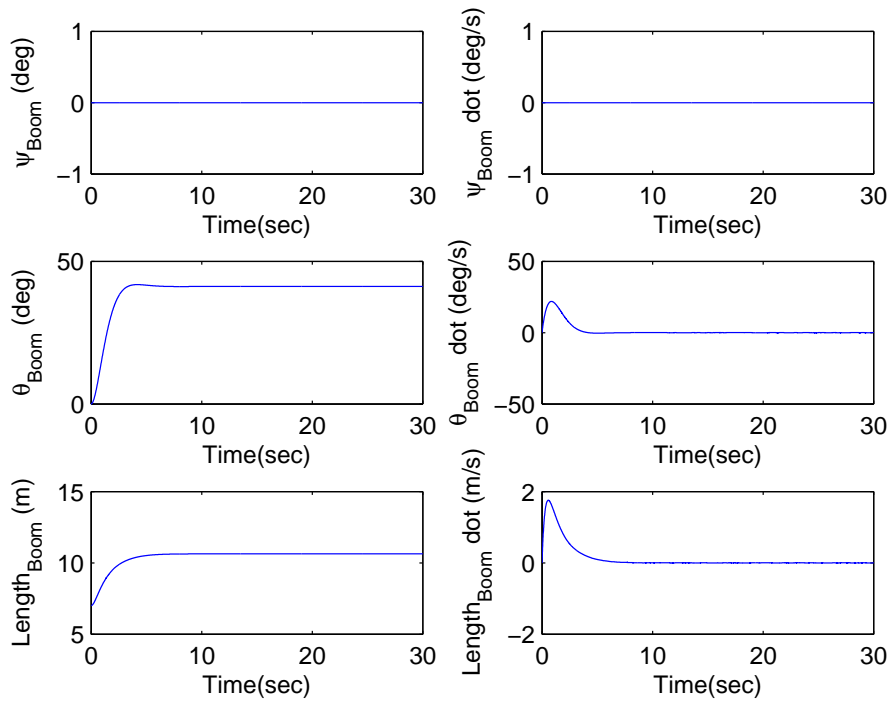Figure 14. Case I Boom Displacement, Rotations, and Rates, Still Air
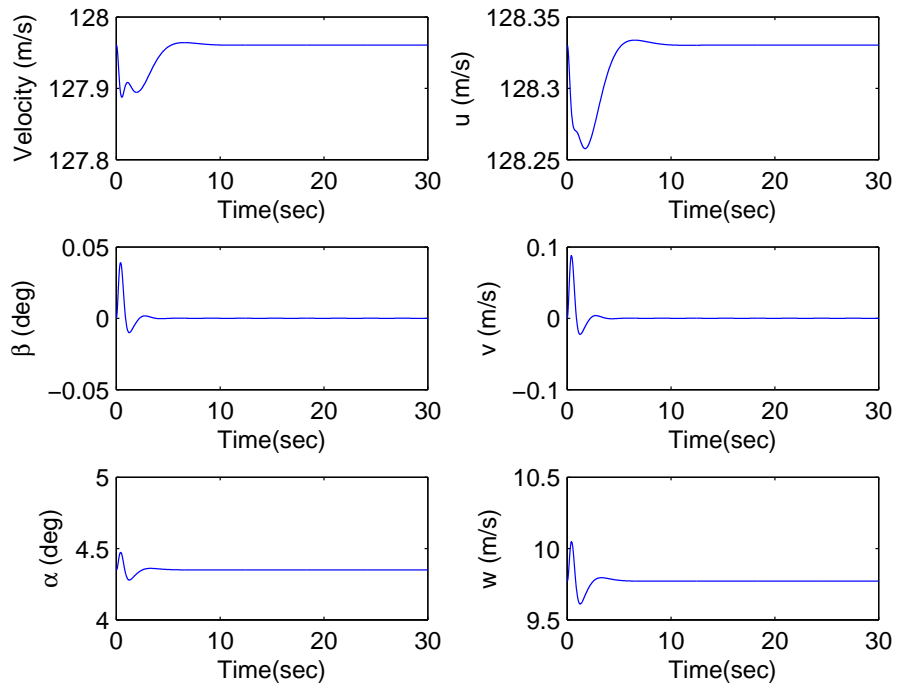
Figure 15. Case I Receiver Aircraft States, Still Air

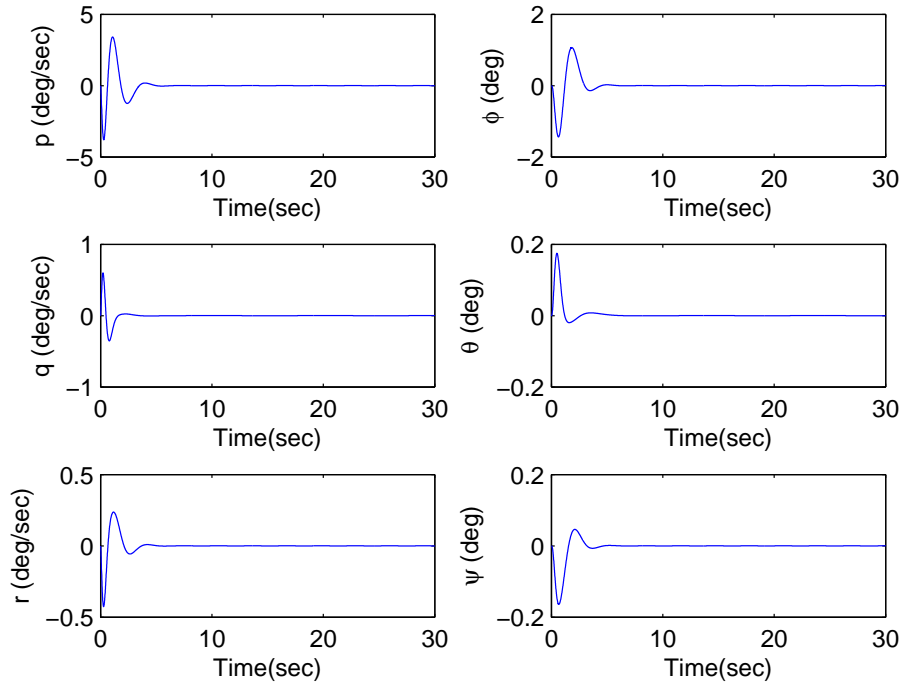American Institute of Aeronautics and Astronautics

Figure 16. Case I Receiver Aircraft Angular States, Still Air
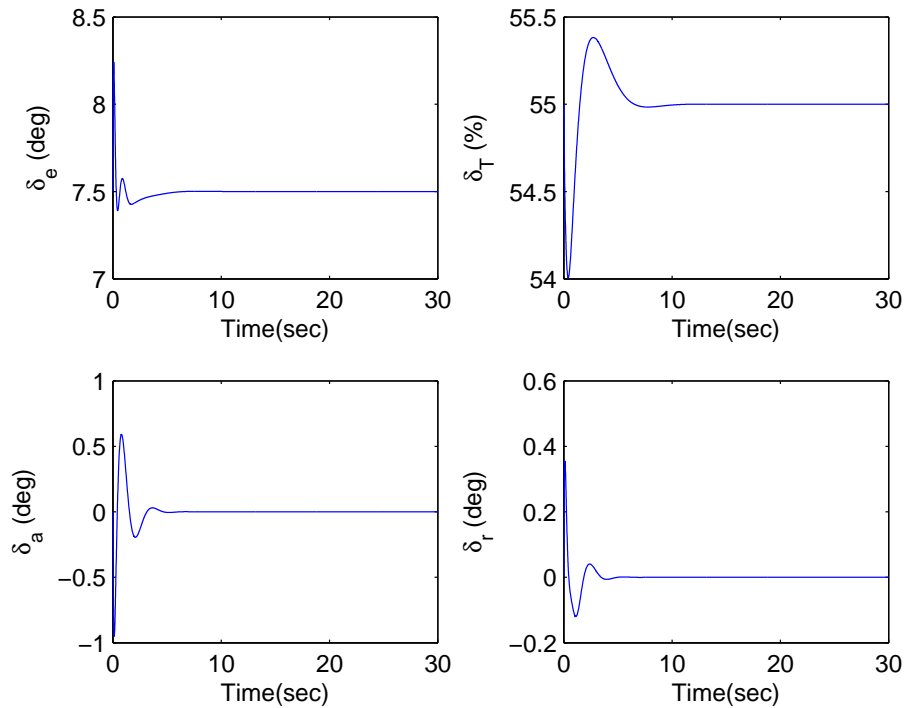
Figure 17. Case I Receiver Aircraft Control Effectors, Still Air

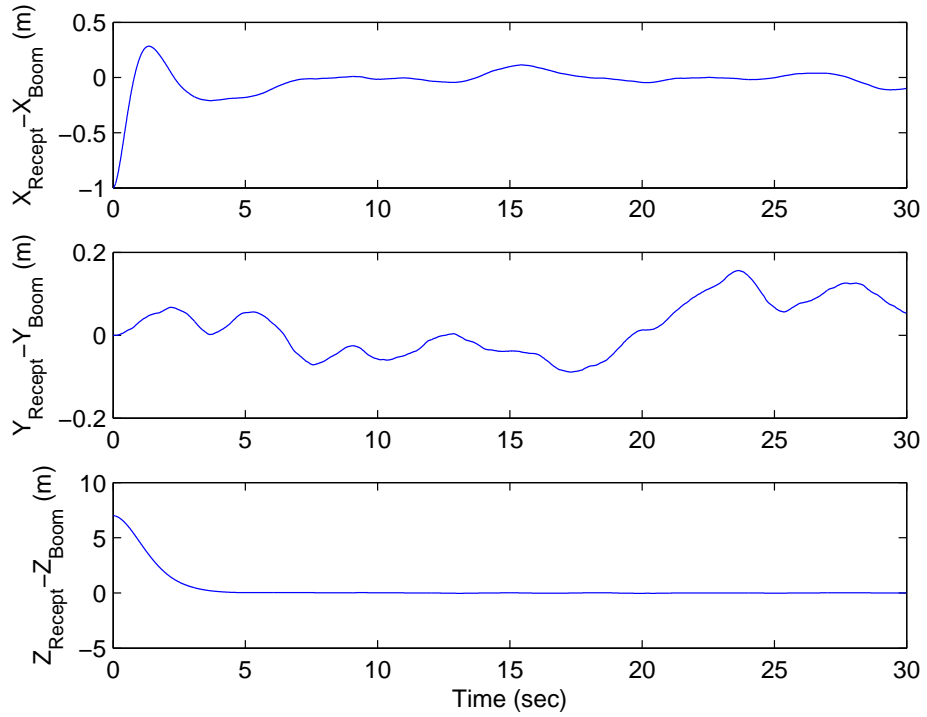American Institute of Aeronautics and Astronautics

Figure 18. Case II Receptacle to Boom Tip Errors, Light Turbulence
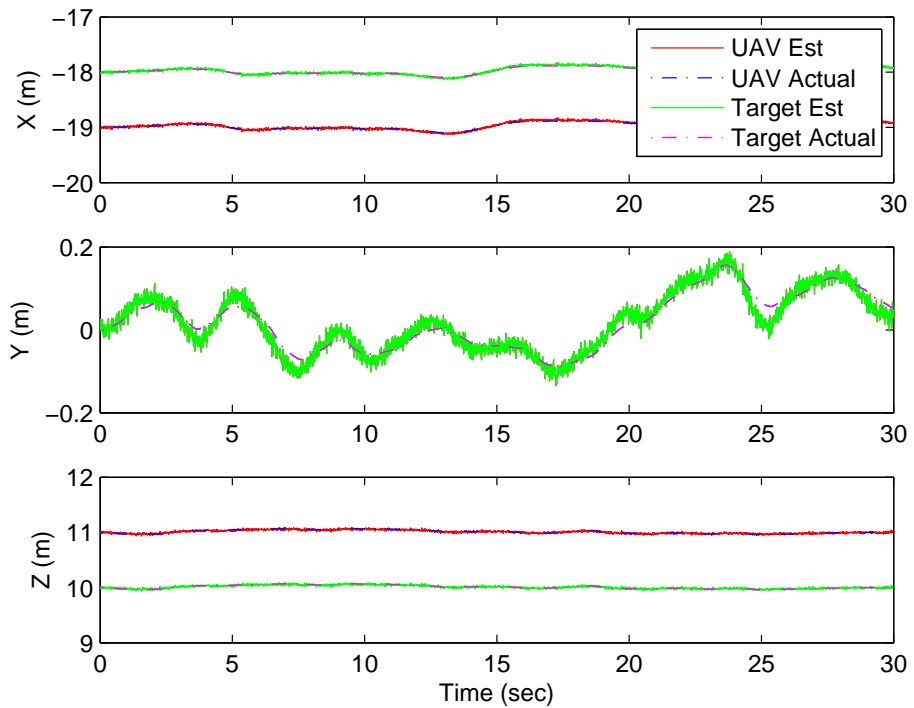
Figure 19. Case II Sensor Output Position Estimates, Light Turbulence
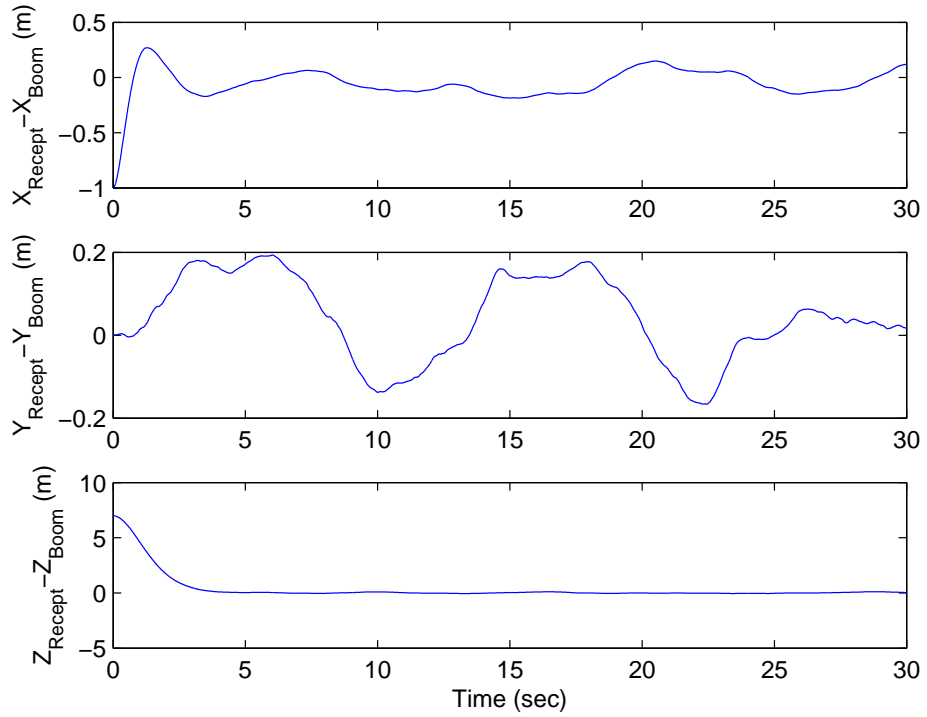
American Institute of Aeronautics and Astronautics

Figure 20. Case III Receptacle to Boom Tip Errors, Moderate Turbulence
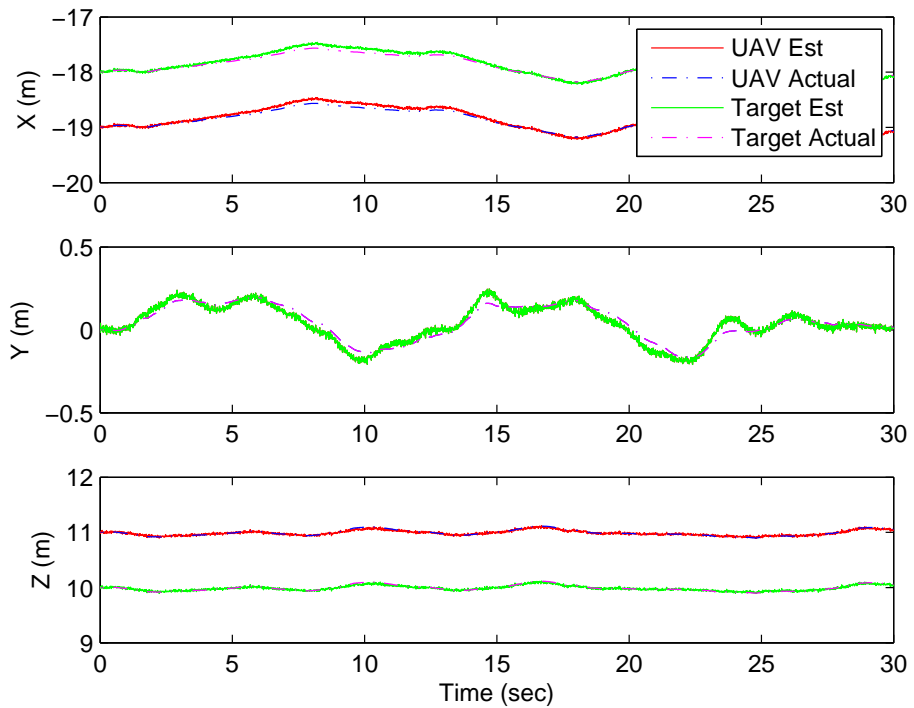
Figure 21. Case III Sensor Output Position Estimates, Moderate Turbulence

American Institute of Aeronautics and Astronautics

Proportional-Integral-Filter Nonzero Set Point methodology, which receives relative position measurements from the optical sensor. Performance and suitability of the system was demonstrated with simulated docking maneuvers between a tanker aircraft and a receiver UAV, in various levels of turbulence. Results indicate that the system is able to successfully accomplish the autonomous refueling task within specifications of docking accuracy and maximum docking velocity. The disturbance accommodation properties of the controller in turbulence are judged to be good, and provide a basis for optimism as regards to proceeding toward actual implementation.

Further investigations will determine the optimal visual target pattern, and determine robustness with respect to off-nominal lighting conditions, additional sensor dynamics, and measurement errors. An improved trajectory tracking controller which can more effectively track time varying receptacle position is being developed in parallel, as a precursor to flight tests.

Acknowledgement

Appendix

The receiver aircraft linear model is obtained by linearizing about steady, level, 1-g trimmed flight. The trim values are angle-of-attack $\alpha_0 = 4.35^o$, trim velocity $V_0 = 128.7$ m/sec, trim elevator deflection $ele_0 = 7.5^o$ and the trim engine power input $pwr_0 = 55\%$. The state vector is

$$x^T = \begin{bmatrix} \delta X & \delta Y & \delta Z & \delta u & \delta v & \delta w & \delta p & \delta q & \delta r & \delta \phi & \delta \theta & \delta \psi \end{bmatrix} \tag{30}$$

$$A = \tag{31}$$

$$\begin{bmatrix}
0 & 0 & 0 & 0.99 & 0 & 0.0759 & 0 & 0 & 0 & 0 & -32.06 & 0 \\
0 & 0 & 0 & 0 & 1 & 0 & 0 & 0 & 0 & -32.06 & 0 & 422.2 \\
0 & 0 & 0 & -0.07 & 0 & 0.99 & 0 & 0 & 0 & 0 & -417.4 & 0 \\
0 & 0 & 0 & -0.03 & 0 & 0.16 & 0 & -31.99 & 0 & 0 & -32.02 & 0 \\
0 & 0 & 0 & 0 & -0.33 & 0 & 31.9 & 0 & -418 & 32.02 & 0 & 0 \\
0 & 0 & 0 & -0.06 & 0 & -1.34 & 0 & 409.5 & 0 & 0 & -2.43 & 0 \\
0 & 0 & 0 & 0 & -0.02 & 0 & -3.64 & 0 & 1.72 & 0 & 0 & 0 \\
0 & 0 & 0 & 0 & 0 & -0.02 & 0 & -0.77 & 0 & 0 & 0 & 0 \\
0 & 0 & 0 & 0 & 0.02 & 0 & -0.21 & 0 & -1.19 & 0 & 0 & 0 \\
0 & 0 & 0 & 0 & 0 & 0 & 1 & 0 & 0.07 & 0 & 0 & 0 \\
0 & 0 & 0 & 0 & 0 & 0 & 0 & 1 & 0 & 0 & 0 & 0 \\
0 & 0 & 0 & 0 & 0 & 0 & 0 & 0 & 1.003 & 0 & 0 & 0
\end{bmatrix}$$

The control vector is

$$\mathbf{u}^T = \begin{bmatrix} \delta ele & \delta\%pwr & \delta ail & \delta rud \end{bmatrix} \tag{32}$$

$$B = \begin{bmatrix} 0 & 0 & 0 & 0 \\ 0 & 0 & 0 & 0 \\ 0 & 0 & 0 & 0 \\ 0.0081 & 0.2559 & 0 & 0 \\ 0 & 0 & -0.2945 & 0.4481 \\ 0.2772 & 0.2286 & 0 & 0 \\ 0 & 0 & 0.5171 & 0.0704 \\ 0.1164 & 0.0143 & 0 & 0 \\ 0 & 0 & 0.0239 & -0.0895 \\ 0 & 0 & 0 & 0 \\ 0 & 0 & 0 & 0 \\ 0 & 0 & 0 & 0 \end{bmatrix} \tag{33}$$

References

[1]Smith, R. K., "Seventy-Five Years of Inflight Refueling," *Air Force and Museums Program*, 1998.

[2]Pennington, R. J., "Tankers," *Air and Space Smithsonian*, Vol. 12, No. 4, November 1997, pp. 24–37.

[3]Maiersperger, W. P., "General Design Aspects of Flight Refueling," *Aeronautical Engineering Review*, Vol. 13, No. 3, March 1954, pp. 52–61.

[4]Personal Conversation with M. Bandak, *Sargent Fletcher Inc.*, Jan 2002.

[5]Stephenson, J. L., *The Air Refueling Receiver That Does Not Complain*, Ph.D. thesis, School of Advanced Airpower Studies Air University, Maxwell Air Force Base, Alabama, June 1998.

[6]Andersen, C. M., *Three Degree of Freedom Compliant Motion Control For Robotic Aircraft Refueling*, Master's thesis, Aeronautical Engineering, Air Force Institute of Technology, Wright-Patterson, Ohio, December 13 1990, AFIT/GAE/ENG/90D-01.

[7]Bennett, R. A., *Brightness Invariant Port Recognition For Robotic Aircraft Refueling*, Master's thesis, Electrical Engineering, Air Force Institute of Technology, Wright-Patterson, Ohio, December 13 1990, AFIT/GE/ENG/90D-04.

[8]Shipman, R. P., *Visual Servoing For Autonomous Aircraft Refueling*, Master's thesis, Air Force Institute of Technology, Wright-Patterson, Ohio, December 1989, AFIT/GE/ENG/89D-48.

[9]Abidi, M. A. and Gonzalez, R. C., "The Use of Multisensor Data for Robotic Applications," *IEEE Transactions on Robotics and Automation*, Vol. 6, No. 2, April 1990, pp. 159–177.

[10]Lachapelle, G., Sun, H., Cannon, M. E., and Lu, G., "Precise Aircraft-to-Aircraft Positioning Using a Multiple Receiver Configuration," *Proceedings of the National Technical Meeting, Institute of Navigation*, Inst of Navigation, Alexandria, VA, 1994, pp. 793–799.

[11]Vendra, S., *Addressing Corner Detection Issues for Machine Vision based UAV*, Master's thesis, College of Engineering and Mineral Resources, West Virginia University, Morgantown, West Virginia, March 2006, Aerospace Engineering Department.

[12]Junkins, J. L., Hughes, D., Wazni, K., and Pariyapong, V., "Vision-Based Navigation for Rendezvous, Docking, and Proximity Operations," *22nd Annual ASS Guidance and Control Conference*, No. ASS-99-021, Breckenridge, Colorado, February 1999.

[13]Alonso, R., Crassidis, J. L., and Junkins, J. L., "Vision-Based Relative Navigation for Formation Flying of Spacecraft," No. AIAA-2000-4439, American Institute of Aeronautics and Astronautics, 2000.

[14]Gunnam, K., Hughes, D., LJunkins, J., and Nasser, K.-N., "A DSP Embedded Optical Navigation System," *Proceedings of the Sixth International Conference on Signal Processing (IC SP '02)*, Beijing, People's Republic of China, August 2002.

[15]Valasek, J., Gunnam, K., Kimmett, J., Tandale, M. D., Junkins, J. L., and Hughes, D., "Vision-Based Sensor and Navigation System for Autonomous Air Refueling," *Journal of Guidance, Control, and Dynamics*, Vol. 28, No. 5, September-October 2005, pp. 832–844.

[16]Tandale, M. D., Bowers, R., and Valasek, J., "Vision-Based Sensor and Navigation System for Autonomous Air Refueling," *Journal of Guidance, Control, and Dynamics*, Vol. 29, No. 4, July-August 2006, pp. 846–857.

[17]Valasek, J., Kimmett, J., Hughes, D., Gunnam, K., and Junkins, J. L., "Vision Based Sensor and Navigation System for Autonomous Aerial Refueling," *Proceedings of the AIAA 1st Technical Conference and Workshop on Unmanned Aerospace Vehicles, Technologies, and Operations*, No. AIAA-2002-3441, Portsmouth, Virgina, May 2002.

[18]Kimmett, J., Valasek, J., and Junkins, J. L., "Autonomous Aerial Refueling Utilizing A Vision Based Navigation System," *Proceedings of the AIAA Guidance, Navigation, and Control Conference*, No. AIAA-2002-4469, Monterey, CA, 5-8 August 2002.

[19]Kimmett, J., Valasek, J., and Junkins, J. L., "Vision Based Controller for Autonomous Aerial

American Institute of Aeronautics and Astronautics

Refueling," *Proceedings of the IEEE Control Systems Society Conference on Control Applications*, No. CCA02-CCAREG-1126, Glasgow, Scotland, Sept. 2002.

[20]Valasek, J. and Junkins, J. L., "Intelligent Control Systems and Vison Based Navigation to Enable Autonomous Aerial Refueling of UAVs," *27th Annual AAS Guidance and Control Conference*, No. AAS 04-012, Breckenridge, CO, Feb. 2004.

[21]Tandale, M. D., Bowers, R., and Valasek, J., "Robust Trajectory Tracking Controller for Vision Based Probe and Drogue Autonomous Aerial Refueling," *Proceedings of the AIAA Guidance, Navigation, and Control Conference*, No. AIAA-2005-5868, San Francisco, CA, 15-18 August 2005.

[22]Tandale, M. D., Valasek, J., and Junkins, J. L., "Vision Based Autonomous Aerial Refueling between Unmanned Aircraft using a Reference Observer Based Trajectory Tracking Controller," *Proceedings of the 2006 American Automatic Control Conference*, No. AIAA-2005-5868, Minneapolis, MN, 14-16 June 2006.

[23]Kass, M., Witkin, A., and Terzopoulos, D., "Snakes: active contour models," *International Journal of Computer Vision*, Vol. 1, No. 4, 1987, pp. 321–331.

[24]Perrin, D. and Smith, C. E., "Rethinking Classical Internal Forces for Active Contour Models," *Proceedings of the IEEE International Conference on Computer Vision and Pattern Recognition*, Vol. 2, Dec. 8–14 2001, pp. 615–620.

[25]Schaub, H. and Smith, C. E., "Color Snakes for Dynamic Lighting Conditions on Mobile Manipulation Platforms," *IEEE/RJS International Conference on Intelligent Robots and Systems*, Las Vegas, NV, Oct. 2003.

[26]Smith, C. E. and Schaub, H., "Efficient Polygonal Intersection Determination with Applications to Robotics and Vision," *IEEE/RSJ International Conference on Intelligent Robots and Systems*, Edmonton, Alberta, Canada, Aug. 2–6 2005.

[27]Monda, M. and Schaub, H., "Spacecraft Relative Motion Estimation using Visual Sensing Techniques," *AIAA Infotech@Aerospace Conference*, Arlington, VA, Sept. 26–29 2005, Paper No. 05-7116.

[28]Kass, M., Witkin, A., and Terzopoulos, D., "Snakes: Active contour models," *International Journal of Computer Vision*, Vol. 1, No. 4, 1987, pp. 321–331.

[29]Perrin, D. P., Ladd, A. M., Kavraki, L. E., Howe, R. D., and Cannon, J. W., "Fast Intersection Checking for Parametric Deformable Models," *SPIE Medical Imaging*, San Diego, CA, February 12–17 2005.

[30]Malladi, R., Kimmel, R., Adalsteinsson, D., Sapiro, G., Caselles, V., and Sethian, J. A., "A geometric approach to segmentation and analysis of 3D medical images," *Proceedings of Mathematical Methods in Biomedical Image Analysis Workshop*, San Francisco, June 21–22 1996.

[31]Ivins, J. and Porrill, J., "Active Region Models for Segmenting Medical Images," *Proceedings of the IEEE International Conference on Image Processing*, Austin, Texas, 1994, pp. 227–231.

[32]Schaub, H. and Wilson, C., "Matching a Statistical Pressure Snake to a Four-Sided Polygon and Estimating the Polygon Corners," Technical Report SAND2004-1871, Sandia National Laboratories, Albuquerque, NM, 2003.

[33]Dorato, P., "Optimal Linear Regulators: The Discrete-Time Case," *IEEE Transactions on Automatic Control*, Vol. AC-16, No. 6, December 1971, pp. 613–620.

[34]Roskam, J., *Airplane Flight Dynamics and Automatic Flight Controls, Part I*, Vol. 1, Design, Analysis, and Research Corporation, Lawrence, KS, 1994, p. 236.